computation

MDPI

Article

Interaction of Hydrogen with Au Modified by Pd and Rh in View of Electrochemical Applications

Fernanda Juarez [1], German Soldano [1], Elizabeth Santos [1,2,*], Hazar Guesmi [3], Frederik Tielens [4,*] and Tzonka Mineva [3,*]

1 Institute of Theoretical Chemistry, Ulm University, Ulm D-89069, Germany; fernanda.juarez@uni-ulm.de (F.J.); gersoldano@gmail.com (G.S.)
2 Facultad de Matemática, Astronomía y Física, Instituto de Física Enrique Gaviola (IFEG-CONICET), Universidad Nacional de Córdoba, Córdoba 5000, Argentina
3 Institut Charles Gerhardt Montpellier, CNRS/ENSCM/UM, 8 rue de l'Ecole normale, Montpellier 34296, France; hazar.guesmi@enscm.fr
4 Sorbonne Universités, UPMC Univ Paris 06, UMR7574 Laboratoire de Chimie de la Matière Condensée de Paris, Collège de France, 11 place Marcelin, Paris F-75005, France
* Correspondence: elisabeth.santos@uni-ulm.de (E.S.); frederik.tielens@upmc.fr (F.T.); tzonka.mineva@enscm.fr (T.M.); Tel.: +49-731-503-1342 (E.S.); +33-1-44-27-56-75 (F.T.); +33-4-67-16-34-68 (T.M.)

Academic Editors: Karlheinz Schwarz and Agnes Nagy
Received: 6 June 2016; Accepted: 13 July 2016; Published: 20 July 2016

Abstract: Hydrogen interaction with bimetallic Au(Pd) and Au(Rh) systems are studied with the density functional theory (DFT)-based periodic approach. Several bimetallic configurations with varying concentrations of Pd and Rh atoms in the under layer of a gold surface(111) were considered. The reactivity of the doped Au(111) toward hydrogen adsorption and absorption was related to the property modifications induced by the presence of metal dopants. DFT-computed quantities, such as the energy stability, the inter-atomic and inter-slab binding energies between gold and dopants, and the charge density were used to infer the similarities and differences between both Pd and Rh dopants in these model alloys. The hydrogen penetration into the surface is favored in the bimetallic slab configurations. The underlayer dopants affect the reactivity of the surface gold toward hydrogen adsorption in the systems with a dopant underlayer, covered by absorbed hydrogen up to a monolayer. This indicates a possibility to tune the gold surface properties of bimetallic electrodes by modulating the degree of hydrogen coverage of the inner dopant layer(s).

Keywords: bimetallic alloy; hydrogen absorption; hydrogen adsorption; gold; DFT; Rh; Pd; dopants

1. Introduction

Catalysts with well-defined heterometallic nanostructures have generated great interest because synergistic effects between different metal atoms can result in enhancement of the catalytic reactivity by tuning the average binding energy of the surface [1–4]. Among bimetallic systems, gold-based alloys are used in a number of catalytic and electrocatalytic reactions, including the direct synthesis of hydrogen peroxide from H_2 and O_2, synthesis of vinyl acetate [5], selective hydrogenation of butadiene [6], etc. Gold nanoparticles with different Pd content were established promising catalysts for CO reforming because of the improved CO oxidation rate [7]. García et al. [8] have shown that Au(Rh) alloy with optimal compositions are three times more reactive than pure Rh catalysts under identical conditions: Rh becomes more reactive when diluted in alloys with Au, even though the latter metal is catalytically inert for the hydrogenation process. The improvement of catalytic activity of nanoalloys originates from two concepts differentiating the bimetallic surfaces from the pure metal: (i) the concept of "ensemble" or strain effect from the size mismatch of the constituent metal atoms;

and (ii) the "ligand" effect from the heterometallic interactions between the surface and substrate metal atoms. The former concept refers to the fact that the addition of a second metal may block certain sites that allow decreasing or eliminating the formation of an undesired intermediate. Thus, specific surface ensembles are required to serve as active sites [5,9].

The adsorbate-induced segregation of metal alloys under the reaction conditions and, thus, the changes in local atomic composition and surface structure have been reported for various bimetallic systems [10–13]. This means that while a given bimetallic configuration may exhibit a desired property, it is important to understand whether the particular configuration is stable under the operating environment for a specific application. Numerous theoretical studies focused on gold bimetallic systems [14–20]. The theoretical results demonstrated that various dopant atoms can organize differently in the alloys, varying from well-dispersed single dopant atoms, to paired or grouped dopants, to well-ordered layers [15]. In our previous work we studied the interaction of hydrogen with a bimetallic system consisting of a complete monolayer of Pd [19,20] underneath the top layer of Au(111). This model was used in a combined density functional and electrocatalysis theory in order to provide a computational protocol for a more quantitative understanding of the mechanisms in electrocatalytic reactions on bimetallic electrodes.

Following this approach we found it of interest to compare the modification of geometric and electronic properties and therefore the reactivity, induced by palladium and rhodium dopants in gold slabs by systematically varying the dopant coverage. This provides an appropriate model to quantitatively investigate the effect of dopants in well-defined Au(Rh) and Au(Pd) structures on the hydrogen adsorption and penetration in the interstitial space between gold and Pd/Rh layers. The dopants are displaced underneath the gold outermost layer that is consistent with the known surface segregation of the noblest element in an alloy under normal conditions, because of its lowest surface energy.

2. Computational Details

All of the computations were performed with plane-wave periodic DFT-based codes Dacapo [21] and VASP [22,23]. The Kohn–Sham equations were solved with the Perdew-Burke-Ernzerhof PBE exchange-correlation functional [17,24], already used in former studies of gold-based systems [17,18,25,26]. The electron-ion interactions, studied with VASP, were described by the projector augmented-wave (PAW) method [27,28]. The electron wave functions were expanded in a plane-wave basis set up to a kinetic energy cutoff of 400 eV. Brillouin zone integration was performed using a $(9 \times 9 \times 1)$ Monkhorst–Pack mesh. In the calculations performed using Dacapo, an energy cutoff of 450 eV and a Monkhorst–Pack grid of $(8 \times 8 \times 1)$ were set [29,30]. The systems are not magnetic, though when the hydrogen atom is farther than 2.2 Å from the surface, it becomes spin polarized. Therefore, spin was only considered for the latter case. The plane wave energy cutoff and the k-point mesh were chosen by optimizing the properties of the bulk systems. The lattice constants calculated from the equilibrium geometry of a periodic fcc bulk structure were 3.83 Å for Rh, 3.99 Å for Pd and 4.18 Å for Au, which are in close agreement with the experimental values 3.80 Å (Rh), 3.89 Å (Pd), and 4.08 Å (Au) [31].

The bimetallic systems were modeled using a slab containing four or six atomic layers of Au(111), separated by a vacuum space with 15 Å thickness. The two bottom layers were constrained at the bulk geometry. Different amounts of gold atoms in the second layer in the Au(111) slab were substituted by Pd and Rh atoms.

The formation energies (ΔE_{form}) of the slabs are calculated using the equation:

$$\Delta E_{\text{form}} = \frac{E_{\text{slab}}(\text{Au}X_n) - E_{\text{slab}}(\text{Au}) + n \cdot E_{\text{bulk}}(\text{Au}) - n \cdot E_{\text{bulk}}(X)}{n} \quad (1)$$

where E_{slab} is the total energy of the slab, E_{bulk} is the total energy of the bulk, X = Pd and Rh, and n is the number of substituted Au atoms by X atoms.

For the study of the hydrogen adsorption and absorption, 1.0 and 0.25 monolayers (ML) coverages were considered. The unit cells used to reproduce these coverages were (1 × 1) and (2 × 2) with one hydrogen atom, respectively. Force tolerance <0.01 eV/Å was set in the geometry optimization computations.

Hydrogen atoms were ad- or absorbed only on surfaces containing one complete monolayer of Pd or Rh. Two types of surfaces were considered: clean and H-precovered surfaces. Therefore, two different definitions of binding energy were used:

$$\Delta E_{\text{bind}} = [E_{\text{alloy+H}} - (E_{\text{alloy}} + 1/2E_{\text{H2}})] \quad (2)$$

$$\Delta E_{\text{bind}} = [E_{\text{preH+H}} - (E_{\text{preH}} + 1/2E_{\text{H2}})] \quad (3)$$

where $E_{\text{alloy+H}}$, E_{alloy}, $E_{\text{preH+H}}$, E_{preH}, and E_{H2}, represent the total energy of the clean surface with and without H, the H-precovered surface, with and without an extra H atom, and the hydrogen molecule in vacuum, respectively.

3. Results and Discussion

3.1. Pd and Rh Induced Structural, Electronic, and Energetic Property Modifications of Au(111)

We first discuss the variation of the structural features of Au(111) because of the various concentrations of Rh and Pd dopants in the sublayers. The considered structures are drawn in Figure 1 and the distances between the layers are plotted in Figure 2 with the following labeling: d_{12} is the distance between the top and the second layers; d_{23} and d_{34} are the separations between the second and the third layers, and the third and the fourth layers, respectively. Comparing these values in the ideal and doped Au(111) slab, it is first noting that the substitution of only one Au atom in the second layer (in the 3 × 3 cell) by Pd and Rh leads to bonding contractions. The Pd impurity has three first gold neighbors at 2.903 Å, whereas Rh-Au distances are 2.888 Å. By consequence the Au-Au distances at the surface layer decrease, as well as the separation between the first and the second layers (d_{12} values in Figure 2) shrinks. The third and fourth layers remain nearly unaffected with d_{23} and d_{34} distances practically equal to those in the undoped gold slab as follows from the results. In all of the cases the distances between Au and Rh atoms are smaller than Pd-Au distances, which is an indication for stronger Au-Rh interactions.

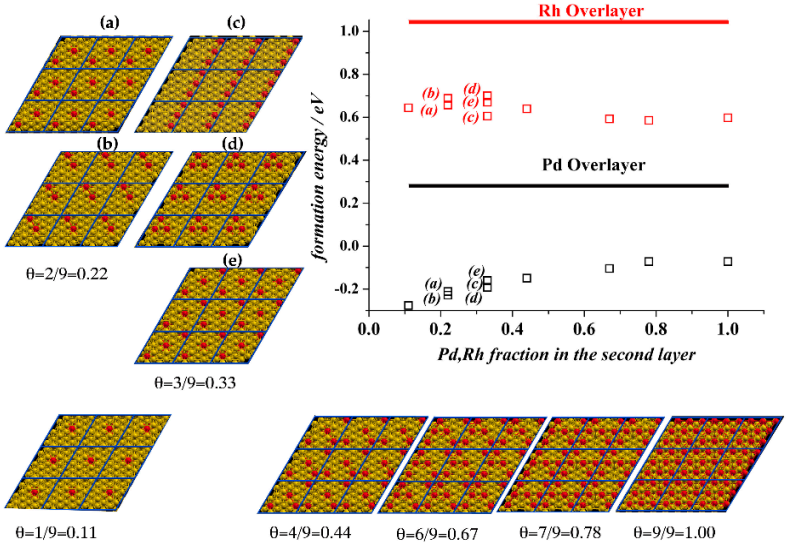

Figure 1. Different modeled fractions of Pd and Rh (ML) in the second layer of Au(111) and their corresponding formation energy (Equation (1)). The (3 × 3) unit cell is shown in blue lines. Gold atoms are presented in yellow spheres. Rh/Pd atoms in the second layer are represented as red spheres.

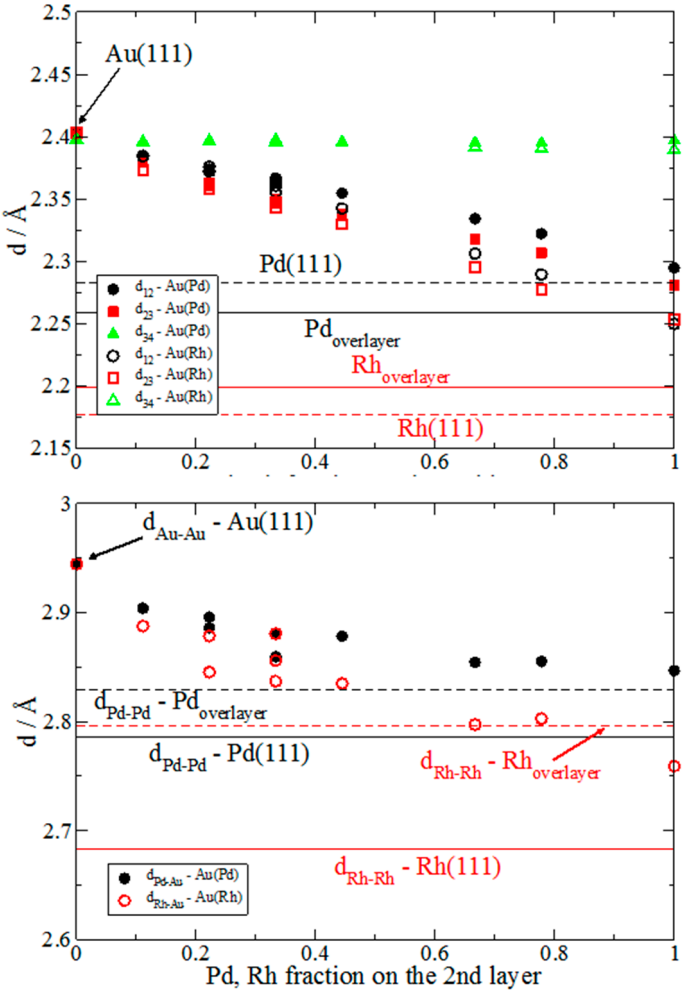

Figure 2. Interlayer separation (**upper**) and Pd-Au or Rh-Au distances (**lower**) as a function of the Pd or Rh fraction in the second layer. All the systems correspond to the ones presented in Figure 1. The (111) surfaces of gold, palladium, and rhodium were used as references. Systems with a complete monolayer of palladium or rhodium on top of gold surfaces were included for sake of comparison.

The computed formation energies, reported also in Figure 1 as an inset, reveal negative ΔE_{form} for Au(Pd) alloy at all the studied concentrations. This means that substituting gold by Pd is energetically favorable. This is in agreement with the phase diagram of the Au-Pd alloy [32] reporting a total miscibility between Au and Pd.

All Rh-substituted structures in Figure 1 are characterized by positive formation energies. This demonstrates that the formation of substituted Rh slabs is endothermic and would not occur spontaneously. Indeed, the Au(Rh) alloy is known for its immiscibility and it is expected to form Rh segregates within Au-solid (phase separation). The preference of Rh atoms to cluster between themselves rather than to coordinate Au atoms can be explained by the cohesive energies in Table 1. Due to the high cohesive energy of Rh compared to that of Pd (-5.77 eV/Å for Rh and -3.72 eV/Å for Pd), the ΔE_{form} of Au(Rh) alloy is positive, while ΔE_{form} for Au(Pd) is negative. As follows from the inset in Figure 1, where ΔE_{form} are plotted versus the increase of the dopants concentration, ΔE_{form} of Au(Rh) does not vary and is nearly constant (within 0.05 eV/atom) with the increase of the sublayer Rh coverage, at variance to the Au(Pd) as discussed above.

Table 1. Unit cell parameter a, cohesive energy ΔE_{coh} and surface energy ΔE_{surf} for the pure bulk metals, Au, Rh, and Pd (distances in Å, ΔE_{coh} in eV/atom, and ΔE_{surf} in eV/Å^2).

	Au	**Rh**	**Pd**
a	4.17	3.84	3.96
a (exp.) [31]	4.08	3.80	3.89
ΔE_{coh}	−2.98	−5.77	−3.72
ΔE_{coh} (exp.) [31]	−3.81	−5.75	−3.89
ΔE_{surf}	0.30	0.87	0.56
ΔE_{surf} (exp.) [33]	0.88	1.1	0.95

The other case of doping distribution in the Au matrix, considered here, are the structures with dopants overlayer. The overlayer formation energies, also reported in the inset in Figure 1 are significantly higher than those computed for the sublayer doped alloys. The overlayer is destabilized by 1.05 and 0.29 eV/atom for Rh and Pd, respectively. This is rather expected, because Au has a lower surface energy than Pd and Rh, and in consequence it tends to segregate at the surface. We can also notice that the segregation energy of a monolayer of Pd from the second to the first layer of the slab, i.e., the energy difference between the system with the Pd-substituted first layer and system with the Pd-substituted second layer is 0.36 eV/atom. This value is similar to the calculated segregation energy of one Pd impurity in the gold matrix [12]. The computed segregation energy of Rh is 0.45 eV/atom, which is in line with the expected trend from the cohesion energies [34].

The bonding between a complete underlayer of Rh or Pd atoms and the gold slab is analyzed by means of the layers' binding energy and electronic density difference. The binding energy between Au and Pd or Rh was calculated from:

$$\Delta E_{bind}(\mathrm{Au-X}) = E_{\mathrm{Au/X/Au(111)}} - E_{\mathrm{Au/vacancy/Au(111)}} - E_{\mathrm{X(2ndL)}} \quad (4)$$

The first term corresponds to the energy of the bimetallic system, being completely relaxed. The second term is the energy of the bimetallic system without the second layer, but with the coordinates of the Au layers fixed to the values obtained relaxing the whole bimetallic system. The third term is the energy of a single Pd or Rh layer with the coordinates fixed to those of the relaxed layer in the bimetallic slab. Table 2 collects the binding energies of Au-Au, Au-Pd, and Au-Rh layers calculated from a pure gold slab, and from a complete underlayer of Pd or Rh, respectively.

Table 2. Binding energies between a gold slab and its second layer, where the second layer can be Pd, Rh, or Au. The former systems correspond to a complete underlayer of Pd or Rh metals on the Au(111) surface and the latter system corresponds to the pure gold surface.

X	ΔE_{bind}**(Au-X)/eV**
Pd	−2.055
Rh	−2.477
Au	−0.973

The bonding energy between the gold layers is higher by 1 eV compared to the binding energies of gold-palladium and gold-rhodium layers. As a possible reason, the increased electronic density between the new metal layer and the gold layers was pointed out [19]. It is worth to note that despite the computed positive formation for the Au(Rh) alloy with an underlayer of Rh (vide supra), the Au-Rh binding between Au-Rh layers is stronger than that between Au-Pd ones. Several reasons for this discrepancy can be pointed out. An increased attraction between Au and X layers is most probably arising from an increased electron density between the two adjacent Au and X layers leading to density depletion between the remaining Au-Au layers, thus rendering the whole slab energetically less stable. Another possible reason could be the effect of the significantly larger cohesive energy of Rh

(−5.8 eV/atom) compared to the cohesive energies of Au and Pd, being almost equal to −3.8 eV/atom (see the computed and experimental [31,33] values in Table 1).

In order to understand whether significant electron density redistribution occurs, to which one can attribute the increased X-Au interactions, we have computed and analyzed the density charge differences, from which the electron density redistribution in the real space can be inferred. The charge differences computed as:

$$\Delta\rho(x,\ y,\ z)_{\text{Au-X}} = \rho_{\text{Au/X/Au(111)}} - \rho_{\text{Au/vacancy/Au(111)}} - \rho_{\text{X(2ndL)}} \quad (5)$$

are shown in Figure 3 for both Pd (left) and Rh (right) underlayers in Au(X) alloys. In Equation (5) $\rho_{\text{Au/X/Au(111)}}$, $\rho_{\text{Au/vacancy/Au(111)}}$, and $\rho_{\text{X(2ndL)}}$ are the spatial electron charge density distributions of the relaxed bimetallic system, the Au(111) system without the second layer of Au with the coordinates fixed to the relaxed bimetallic system, and the isolated second layer of Pd or Rh with the coordinates of Pd or Rh in the bimetallic system.

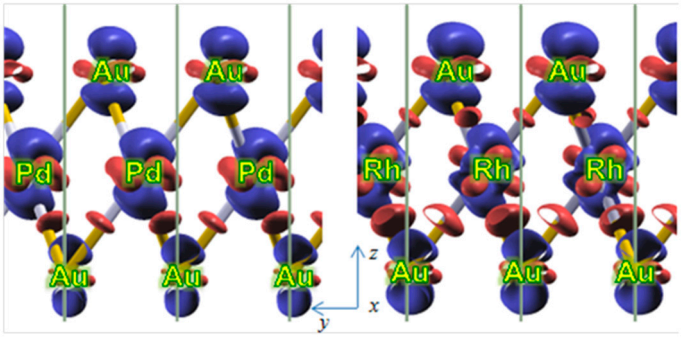

Figure 3. Charge density difference after the formation of a whole underlayer of Pd (**left**) and Rh (**right**) below the surface of Au(111) slab as obtained from Equation (5). Isosurface equal to 0.004 e· Å^{-3}. Red and blue colors correspond to electron accumulation and depletion, respectively.

This analysis reveals a charge depletion along *z*-direction at both Au and X sites and a charge accumulation in the *xy*-plane at the atomic sites as well as along the X-Au (inner, third Au- layer) bonds. Therefore, a charge distribution from *z*- toward *xy*-plane occurred because of the Au-substitution by Pd and Rh. The picture is similar for Pd and Rh layers, although a slightly higher charge accumulation along Rh-Au bonds is observed. There is not a charge accumulation between the surface gold layer and the Pd layer at variance to the Rh-Au (Au surface layer). The withdrawal of electron density toward gold atoms is explained by the higher Au electronegativity than that of Pd and Rh. The larger charge accumulation found for Rh-Au bonds favors the Au-Rh interlayer binding compared to the Pd-Au one. This agrees as well with the shorter Rh-Au than Pd-Au distances reported in Figure 2. The charge density redistribution is observed only for the adjacent Au-X layers and not for the Au-Au layers (see Figure 3). It follows that the dopants cause only locally a density drift from *z*- to *xy*- plane. This is the most likely reason for the gold-dopant layer stabilization and inter-atomic, and inter-layer geometrical modifications (vide supra) in the doped gold slab compared to the pure Au(111). The local in space electron density reorganization affects predominantly the adjacent dopant-gold layers and not the remaining gold layers in the gold slab.

3.2. Hydrogen Ab- and Adsorption

To study the reactivity of the doped Au(111) slab, hydrogen ab- and adsorption reactions were considered for the Au-X systems with a complete X monolayer underneath the Au-surface layer. For comparison, the hydrogen interaction with undoped Au(111) is also considered. Many previous investigations devoted to hydrogen ab- and adsorption on ideal monometallic surfaces, including Au(111), provided already sound information [35–39]. Concerning the most favored adsorption sites,

there is a general consensus that H adsorbs preferably on both hexagonal closed packed (hcp) and face-centered cubic (fcc) three-fold hollow sites on a large variety of metal surfaces. In this study we will also consider hcp and fcc sites because the absorption process should be different for H atoms diffusing to subsurfaces from both slab sites. To characterize different sites, first the adsorption energies of H atoms on top of the monometallic Rh, Pd, and Au surfaces were computed and are collected in Table 3. Our results are in very good agreement with those reported previously [36,38,39].

Table 3. Binding energy ΔE_{bind} of hydrogen adsorbed on mono- and bimetallic surfaces, calculated according to Equations (2) and (3). Hydrogen atoms ad- and absorbed on these surfaces are labeled H_s and H_{ss}, respectively. The binding energy was only calculated for the adsorbed H_s atoms. The labels Au(Rh) and Au(Pd) correspond to a Rh or Pd complete monolayer (ML) in the Au(111) slab, respectively. The energies are in eV.

		θ(H_s) = 0.25 ML		**θ(H_s) = 1.00 ML**	
		fcc	**hcp**	**fcc**	**hcp**
Pd(111)		−0.61			
Rh(111)		−0.56			
Au(111)		0.10			
Clean surfaces (θ(H_{ss}) = 0.00 ML)	Au(Pd)	0.10	0.17	0.27	0.31
	Au(Rh)	0.01	0.11	0.20	0.27
Surfaces containing H (θ(H_{ss}) = 0.25 ML)	Au(Pd)	(A) 0.10	0.19		
		(B) 0.15	0.24		
	Au(Rh)	(A) 0.01	0.12		
		(B) 0.04	0.20		
Surfaces containing H (θ(H_{ss}) = 1.00 ML)	Au(Pd)	0.007	0.03	0.18	0.18
	Au(Rh)	0.01	0.08	0.20	0.23

The hydrogen atoms adsorbed on the surface gold atoms ($z_H > z_{Au\_top\_layer}$) are labeled as H_s and those bound to the atoms of the underlying second layer (H-absorption; $z_H < z_{Au\_top\_layer}$) are labeled as H_{ss}. The computed binding energies for the ad- and absorption of one H atom are presented in Tables 3 and 4, respectively. The adsorption energies on the bimetallic systems (without pre-absorbed H_{ss} underneath the surface) are the same as on the pure gold surface, within the DFT error. There is only a small decrease in the energy (and an increase in the bond length) in the Au(Rh) slab. When the H-coverage is increased, the H binding energies decrease. At low hydrogen coverage, the H-interaction with the second layer atoms (H-absorption) is higher than E_{ads} that indicates that H-penetration into the interstitial space is favored compared to the surface adsorption. The latter result is expected because H in the second layer interacts with three Pd or Rh dopant atoms and only one Au atom. It is, thus, not surprising that the interaction with the surface gold atoms remains weaker. Nevertheless those surface atoms are bound to the dopants in the second layer. This is in line with the above-discussed result that there is not an important charge drift in Au_{surf}-X bond region, contrary to the charge accumulation in the X-Au (3rd layer) space (see Figure 3).

Table 4. Binding energy ΔE_{bind} of hydrogen absorbed on mono- and bimetallic surfaces, calculated according to Equation (2). The binding energy was only calculated for the absorbed hydrogen atoms, labeled as H_{ss}. The labels Au(Rh) and Au(Pd) correspond to a Rh or Pd complete monolayer in the Au(111) slab, respectively. The energies are in eV.

		$\theta(H_{ss})$ = 0.25 ML		$\theta(H_{ss})$ = 1.00 ML	
		fcc	**hcp**	**fcc**	**hcp**
Pd(111)		−0.28			
Rh(111)		0.18			
Au(111)		0.89			
Clean surfaces ($\theta(H_{ss})$ = 0.00 ML)	Au(Pd)	−0.17	0.36	0.05	0.51
	Au(Rh)	−0.40	0.25	−0.31	0.41

In addition to the minima structures, the effect of dopants on the hydrogen absorption energy was studied. The saddle points on the PES were localized by using the nudge elastic band technique as implemented in the VASP code. Figure 4 shows the potential energy of hydrogen penetrating the alloy as a function of the z-coordinates of the hydrogen. The reaction and activation energies are collected in Table 5. The activation energy for hydrogen absorption is 0.42 eV for Au(Rh) and 0.33 eV for Au(Pd), which is of the same order of magnitude as that on Pd(111) (see Table 5). This is perfectly in line with the computed stronger Rh-Au bond energies (Table 2), indicating that a strongly bound Rh to Au would rend the Au-Rh dimer less reactive.

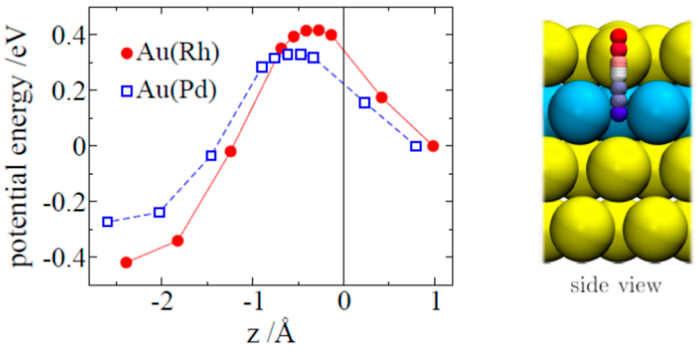

Figure 4. Potential energy for a hydrogen absorption process as a function of the hydrogen distance from the surface (z). The energy reference corresponds to the adsorption of hydrogen in the hollow-fcc site. The corresponding snapshots of the process are shown at the right hand side.

Table 5. Reaction and activation energy for hydrogen diffusion from the surface (s) to the subsurface (ss) and vice versa on the bimetallic systems (Au(Pd) and Au(Rh)) in comparison with previous calculations of the literature for Pd(111) and Au(111) [39]. All values are in eV.

	$\Delta E(H_s \rightarrow H_{ss})$	$E_{act}(H_s \rightarrow H_{ss})$	$E_{act}(H_{ss} \rightarrow H_s)$
Pd(111)	0.30	0.40	0.10
Rh(111)	0.76	0.84	0.09
Au(111)	0.64	0.76	0.12
Au(Pd)	−0.26	0.33	0.59
Au(Rh)	−0.41	0.42	0.83

We also studied the desorption process and found a significantly higher activation barrier (>0.6 eV), which demonstrates that the absorbed hydrogen would be hardly evacuated from the underneath layers. Further on, by comparing the adsorption energies on clean bimetallic surfaces ($\theta(H_{ss})$ = 0.00) and on pre-H-covered surfaces ($\theta(H_{ss})$ = 0.25, or 1.00), it appears that the effect of the

underneath hydrogen atoms is weak. The 0.25 ML hydrogen precovered underlayer structures are shown in Figure 5. Nevertheless, an increase in the bond strength (or a decrease in the adsorption energy) is observed for a complete layer of hydrogen atoms under the surface. This suggests that by changing the degree of hydrogen coverage one can modify the gold surface reactivity toward interaction with hydrogen and, thus modifying the reactivity of the bimetallic gold-covered electrodes.

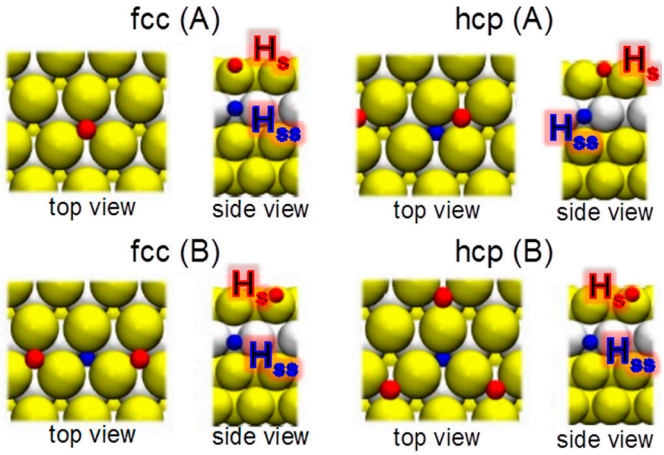

Figure 5. Top and side views for small coverages of the adsorbed and absorbed hydrogen ($\theta(H_{ss})$ =0.25, $\theta(H_s)$ = 0.25).

Finally, the change in the work functions at high coverage was calculated and the results are reported in Table 6. As expected the adsorption of hydrogen lowers the work function of the surface, whereas absorption increases it. When hydrogen atoms are located in/on the alloy surface the work function is lower and similar to that of the work function of the system with adsorbed hydrogen.

Table 6. Delta work function $\Delta\Phi$ for single hydrogen ab/adsorption and for both species simultaneously. In each case the reference is the work function of the corresponding clean alloy surface. All the values are in eV.

$\theta(H_{ss})$ (ML)	$\theta(H_s)$ (ML)	Site	Au(Rh)	Au(Pd)
0.00	1.00	fcc	−0.43	−0.41
		hcp	−0.32	−0.32
1.00	0.00	fcc	0.25	0.35
		hcp	0.27	0.16
1.00	1.00	fcc	−0.36	−0.45
		hcp	−0.33	−0.44

4. Conclusions

Structural variations, energetics, and density of charge differences are studied with periodic DFT for a series of Au(Rh) and Au(Pd) alloy models as a function of Rh/Pd dopant concentration. The interaction of these bimetallic systems with hydrogen was investigated through computations of the adsorption and absorption energies of hydrogen, as well as the activation energies for the H-absorption reactions.

Positive formation energies are found for all Au(Rh) slab models, whereas the formation energies of Au(Pd) are negative, indicating a miscibility between Pd and Au. Dopants were placed in the second (underlayer) below the gold surface and induced shrinking of the interatomic distances between the gold surface atoms. This is most probably caused by the lattice mismatch, rather than by electron structure modifications, because only an insignificant charge density variation is obtained in the space

between the gold atoms at the surface and the Pd/Rh underlayers. The latter suggestion is corroborated by the very similar hydrogen adsorption energies found for the pure Au(111) and bimetallic slabs with an underneath Pd/Rh layer. The H-penetration (absorption) is better stabilized in the bimetallic alloys, because of the stronger Pd-H/Rh-H interactions in the second layers than the Au-H binding at the surface without dopants. In structures with a full dopant underlayer, covered by a hydrogen monolayer, the H-adsorption at the surface gold atoms decreases. This suggests that the reactivity of the gold surface in bimetallic alloys can be tuned by varying the hydrogen coverage.

Acknowledgments: This work is part of the research network financed by the Deutsche Forschungsgemeinschaft FOR1376 and the DAAD-PHC PROCOPE 2011 PROJECT N 25099UB. E.S. acknowledges PIP-CONICET 112-201001-00411 and PICT-2012-2324 (Agencia Nacional de Promoción Científica y Tecnológica, FONCYT, préstamo BID). The calculations were carried out on the HPC resources from GENCI-[CCRT/CINES/IDRIS] (Grant 2016-[x2016087369]) and the CCRE of Université Pierre et Marie Curie.

Author Contributions: E.S. and F.T. conceived and designed the computations; F.J. and G.S. carried out the calculations and contributed to the data analysis; H.G. analyzed the data; T.M. wrote the paper with inputs from all the authors.

Conflicts of Interest: The authors declare no conflict of interest.

References

1. Liu, J.H.; Wang, A.Q.; Chi, Y.S.; Lin, H.P.; Mou, C.Y. Synergistic Effect in an Au-Ag Alloy Nanocatalyst: Co Oxidation. *J. Phys. Chem. B* **2005**, *109*, 40–43. [CrossRef] [PubMed]
2. Wang, D.; Villa, A.; Porta, F.; Prati, L.; Su, D. Bimetallic Gold/Palladium Catalysts: Correlation between Nanostructure and Synergistic Effects. *J. Phys. Chem. C* **2008**, *112*, 8617–8622. [CrossRef]
3. Mott, D.; Luo, J.; Njoki, P.N.; Lin, Y.; Wang, L.; Zhong, C.-J. Synergistic Activity of Gold-Platinum Alloy Nanoparticle Catalysts. *Catal. Today* **2007**, *122*, 378–385. [CrossRef]
4. Zhang, L.; Iyyamperumal, R.; Yancey, D.F.; Crooks, R.M.; Henkelman, G. Design of Pt-Shell Nanoparticles with Alloy Cores for the Oxygen Reduction Reaction. *ACS Nano* **2013**, *7*, 9168–9172. [CrossRef] [PubMed]
5. Chen, M.S.; Kumar, D.; Yi, C.W.; Goodman, D.W. The Promotional Effect of Gold in Catalysis by Palladium-Gold. *Science* **2005**, *310*, 291–293. [CrossRef] [PubMed]
6. Hugon, A.; El Kolli, N.; Louis, C. Advances in the Preparation of Supported Gold Catalysts: Mechanism of Deposition, Simplification of the Procedures and Relevance of the Elimination of Chlorine. *J. Catal.* **2010**, *274*, 239–250. [CrossRef]
7. Gao, F.; Wang, Y.; Goodman, D.W. Co Oxidation over Aupd(100) from Ultrahigh Vacuum to near-Atmospheric Pressures: The Critical Role of Contiguous Pd Atoms. *J. Am. Chem. Soc.* **2009**, *131*, 5734–5735. [CrossRef] [PubMed]
8. Garcia, S.; Zhang, L.; Piburn, G.W.; Henkelman, G.; Humphrey, S.M. Microwave Synthesis of Classically Immiscible Rhodium-Silver and Rhodium-Gold Alloy Nanoparticles: Highly Active Hydrogenation Catalysts. *ACS Nano* **2014**, *8*, 11512–11521. [CrossRef] [PubMed]
9. Garcia-Mota, M.; Lopez, N. The Role of Long-Lived Oxygen Precursors on Aum Alloys (M = Ni, Pd, Pt) in Co Oxidation. *Phys. Chem. Chem. Phys.* **2011**, *13*, 5790–5797. [CrossRef] [PubMed]
10. Tenney, S.A.; He, W.; Roberts, C.C.; Ratliff, J.S.; Shah, S.I.; Shafai, G.S.; Turkowski, V.; Rahman, T.S.; Chen, D.A. Co-Induced Diffusion of Ni Atoms to the Surface of Ni-Au Clusters on Tio2(110). *J. Phys. Chem. C* **2011**, *115*, 11112–11123. [CrossRef]
11. Guesmi, H.; Louis, C.; Delannoy, L. Chemisorbed Atomic Oxygen Inducing Pd Segregation in Pdau(111) Alloy: Energetic and Electronic DFT Analysis. *Chem. Phys. Lett.* **2011**, *503*, 97–100. [CrossRef]
12. Dhouib, A.; Guesmi, H. DFT Study of the M Segregation on Mau Alloys (M = Ni, Pd, Pt) in Presence of Adsorbed Oxygen O and O_2. *Chem. Phys. Lett.* **2012**, *521*, 98–103. [CrossRef]
13. Pittaway, F.; Paz-Borbon, L.O.; Johnston, R.L.; Arslan, H.; Ferrando, R.; Mottet, C.; Barcaro, G.; Fortunelli, A. Theoretical Studies of Palladium-Gold Nanoclusters: Pd-Au Clusters with up to 50 Atoms. *J. Phys. Chem. C* **2009**, *113*, 9141–9152. [CrossRef]
14. Guesmi, H. Theoretical Insights on the Effect of Reactive Gas on the Chemical Ordering of Gold-Based Alloys. *Gold Bull.* **2013**, *46*, 213–219. [CrossRef]

15. Zhu, B.; Guesmi, H.; Creuze, J.; Legrand, B.; Mottet, C. Crossover among Structural Motifs in Pd-Au Nanoalloys. *Phys. Chem. Chem. Phys.* **2015**, *17*, 28129–28136. [CrossRef] [PubMed]
16. Ferrando, R.; Jellinek, J.; Johnston, R.L. Nanoalloys: From Theory to Applications of Alloy Clusters and Nanoparticles. *Chem. Rev.* **2008**, *108*, 845–910. [CrossRef] [PubMed]
17. Visart de Bocarme, T.; Chau, T.D.; Tielens, F.; Andres, J.; Gaspard, P.; Wang, R.L.C.; Kreuzer, H.J.; Kruse, N. Oxygen Adsorption on Gold Nanofacets and Model Clusters. *J. Chem. Phys.* **2006**, *125*, 054703. [CrossRef] [PubMed]
18. Tielens, F.; Andrés, J.; Chau, T.-D.; Visart de Bocarmé, T.; Kruse, N.; Geerlings, P. Molecular Oxygen Adsorption on Electropositive Nano Gold Tips. *Chem. Phys. Lett.* **2006**, *421*, 433–438. [CrossRef]
19. Juarez, M.F.; Soldano, G.; Guesmi, H.; Tielens, F.; Santos, E. Catalytic Properties of Au Electrodes Modified by an Underlayer of Pd. *Surf. Sci.* **2015**, *631*, 235–247. [CrossRef]
20. Quaino, P.M.; Nazmutdinov, R.; Peiretti, L.F.; Santos, E. Unravelling the Hydrogen Absorption Process in Pd Overlayers on a Au(111) Surface. *Phys. Chem. Chem. Phys.* **2016**, *18*, 3659–3668. [CrossRef] [PubMed]
21. Hammer, B.; Hansen, L.B.; Norskov, J.K. Improved Adsorption Energetics within Density-Functional Theory Using Revised Perdew-Burke-Ernzerhof Functionals. *Phys. Rev. B* **1999**, *59*, 7413–7421. [CrossRef]
22. Kresse, G.; Hafner, J. Ab-Initio Molecular-Dynamics for Liquid-Metals. *Phys. Rev. B* **1993**, *47*, 558–561. [CrossRef]
23. Kresse, G.; Hafner, J. Ab-Initio Molecular-Dynamics Simulation of the Liquid-Metal Amorphous-Semiconductor Transition in Germanium. *Phys. Rev. B* **1994**, *49*, 14251–14269. [CrossRef]
24. Perdew, J.P.; Chevary, J.A.; Vosko, S.H.; Jackson, K.A.; Pederson, M.R.; Singh, D.J.; Fiolhais, C. Atoms, Molecules, Solids, and Surfaces: Applications of the Generalized Gradient Approximation for Exchange and Correlation. *Phys. Rev. B* **1992**, *46*, 6671–6687. [CrossRef]
25. Tielens, F.; Andres, J. Prediction of Gold Zigzag Nanotube-Like Structure Based on Au-32 Units: A Quantum Chemical Study. *J. Phys. Chem. C* **2007**, *111*, 10342–10346. [CrossRef]
26. Rodriguez-Castillo, M.; Laurencin, D.; Tielens, F.; van der Lee, A.; Clement, S.; Guari, Y.; Richeter, S. Reactivity of Gold Nanoparticles Towards N-Heterocyclic Carbenes. *Dalton Trans.* **2014**, *43*, 5978–5982. [CrossRef] [PubMed]
27. Perdew, J.P.; Burke, K.; Ernzerhof, M. Generalized Gradient Approximation Made Simple. *Phys. Rev. Lett.* **1996**, *77*, 3865–3868. [CrossRef] [PubMed]
28. Perdew, J.P.; Burke, K.; Ernzerhof, M. Generalized Gradient Approximation Made Simple (Vol 77, Pg 3865, 1996). *Phys. Rev. Lett.* **1997**, *78*, 1396–1396. [CrossRef]
29. Blochl, P.E.; Jepsen, O.; Andersen, O.K. Improved Tetrahedron Method for Brillouin-Zone Integrations. *Phys. Rev. B* **1994**, *49*, 16223–16233. [CrossRef]
30. Monkhorst, H.J.; Pack, J.D. Special Points for Brillouin-Zone Integrations. *Phys. Rev. B* **1976**, *13*, 5188–5192. [CrossRef]
31. Kittel, C. *Introduction to Solid State Physics*, 3rd ed.; Wiley: New York, NY, USA, 1967.
32. Sluiter, M.H.F.; Colinet, C.; Pasturel, A. Ab Initio Calculation of the Phase Stability in Au-Pd and Ag-Pt Alloys. *Phys. Rev. B* **2006**, *73*, 174204. [CrossRef]
33. Skriver, H.L.; Rosengaard, N.M. Surface Energy and Work Function of Elemental Metals. *Phys. Rev. B Condens. Matter Mater. Phys.* **1992**, *46*, 7157–7168. [CrossRef]
34. Yanagita, H.; Fujioka, H.; Aruga, T.; Takagi, N.; Nishijima, M. Vibrational Spectra of Hydrogen on the Rh(111) Surface. *Surf. Sci.* **1999**, *441*, 507–514. [CrossRef]
35. Mann, S.S.; Seto, T.; Barnes, C.J.; King, D.A. Coverage Dependence of Surface-Diffusion of Hydrogen and Deuterium on Rh(111) by Laser-Induced Thermal-Desorption. *Surf. Sci.* **1992**, *261*, 155–163. [CrossRef]
36. Soldano, G.; Schulz, E.N.; Salinas, D.R.; Santos, E.; Schmickler, W. Hydrogen Electrocatalysis on Overlayers of Rhodium over Gold and Palladium Substrates-More Active Than Platinum? *Phys. Chem. Chem. Phys.* **2011**, *13*, 16437–16443. [CrossRef] [PubMed]
37. Wilke, S.; Natoli, V.; Cohen, M.H. Theoretical Investigation of Water Formation on Rh and Pt Surfaces. *J. Chem. Phys.* **2000**, *112*, 9986–9995. [CrossRef]
38. Quaino, P.; Santos, E.; Wolfschmidt, H.; Montero, M.A.; Stimming, U. Theory Meets Experiment: Electrocatalysis of Hydrogen Oxidation/Evolution at Pd-Au Nanostructures. *Catal. Today* **2011**, *177*, 55–63. [CrossRef]

39. Ferrin, P.; Kandoi, S.; Nilekar, A.U.; Mavrikakis, M. Hydrogen Adsorption, Absorption and Diffusion on and in Transition Metal Surfaces: A DFT Study. *Surf. Sci.* **2012**, *606*, 679–689. [CrossRef]